Supporting Information

Boosting the Performance of One-Step Solution-Processed Perovskite Solar Cells using a Natural Monoterpene Alcohol as Green Solvent Additive

*Giuliana Giuliano,[a] Aurelio Bonasera,[a,b] Michelangelo Scopelliti,[a,b,c] Delia Chillura Martino,[b,d] Tiziana Fiore,[a,c] and Bruno Pignataro[a,b]**

[a]Department of Physics and Chemistry - Emilio Segrè, University of Palermo, Viale delle Scienze, bld. 17, 90128 Palermo, Italy

[b]INSTM – Palermo Research Unit, Viale delle Scienze, bld. 17, 90128 Palermo, Italy

[c]Consorzio Interuniversitario di Ricerca in Chimica dei Metalli nei Sistemi Biologici (C.I.R.C.M.S.B.), Piazza Umberto I, 1, 70121 Bari, Italy

[d]Department of Biological, Chemical, and Pharmaceutical Sciences and Technologies (STeBiCeF), University of Palermo, Viale delle Scienze, bld. 17, 90128 Palermo, Italy

[*]E-mail: bruno.pignataro@unipa.it

Keywords: perovskite solar cells; additives; solvent engineering; terpineol; alcohol; green; one-step deposition.

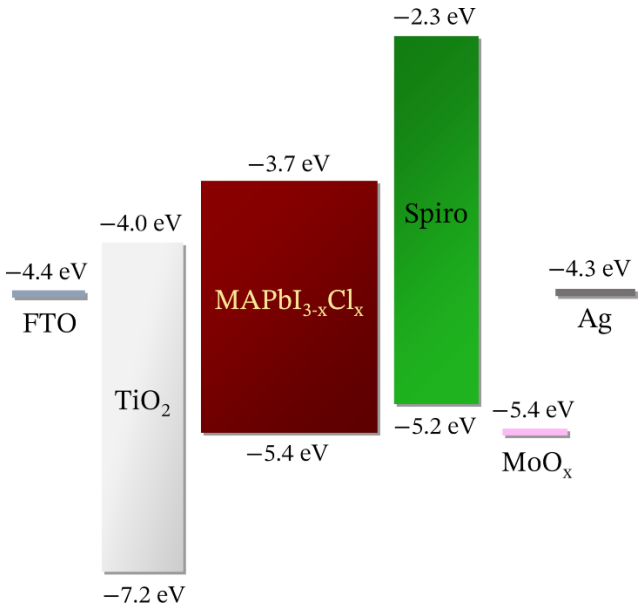

Figure S1. Energy band diagram of the complete planar n-i-p perovskite solar cell. Literature reports for band edges and Fermi levels were used.[1–3]

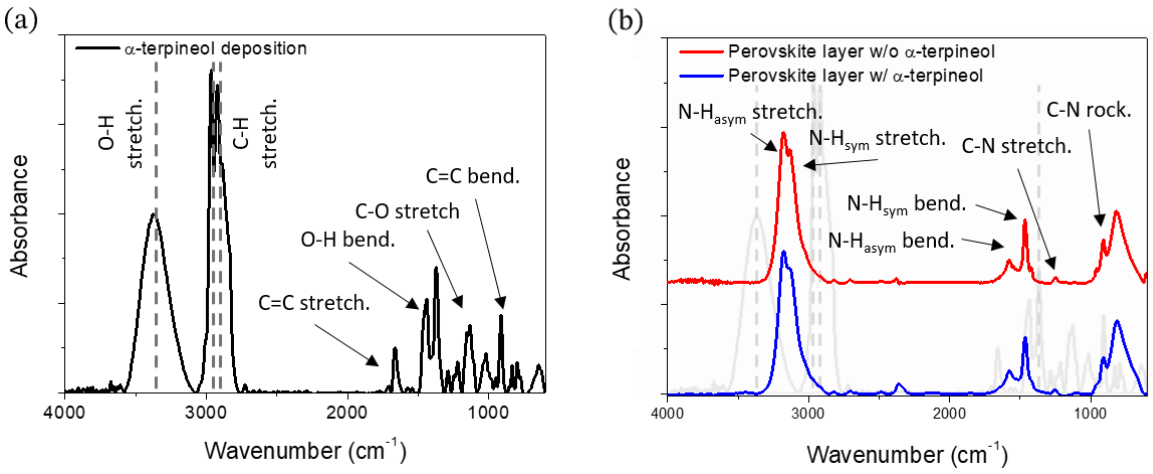

Figure S2. FT-IR spectra registered for: (a) a deposition of a 10 vol% solution of α-terpineol in chloroform over a glass support, left to dry under air at room temperature, and (b) a perovskite layer grown in absence (**red line**) and presence (**blue line**) of α-terpineol prepared in accordance with the general procedure reported in Experimental Section in the main text. For the latter spectrum, the absence of pure α-terpineol band (in the background) supports the hypothesis of a

successful removal of the additive when the perovskite layer has been grown in presence of the additive.

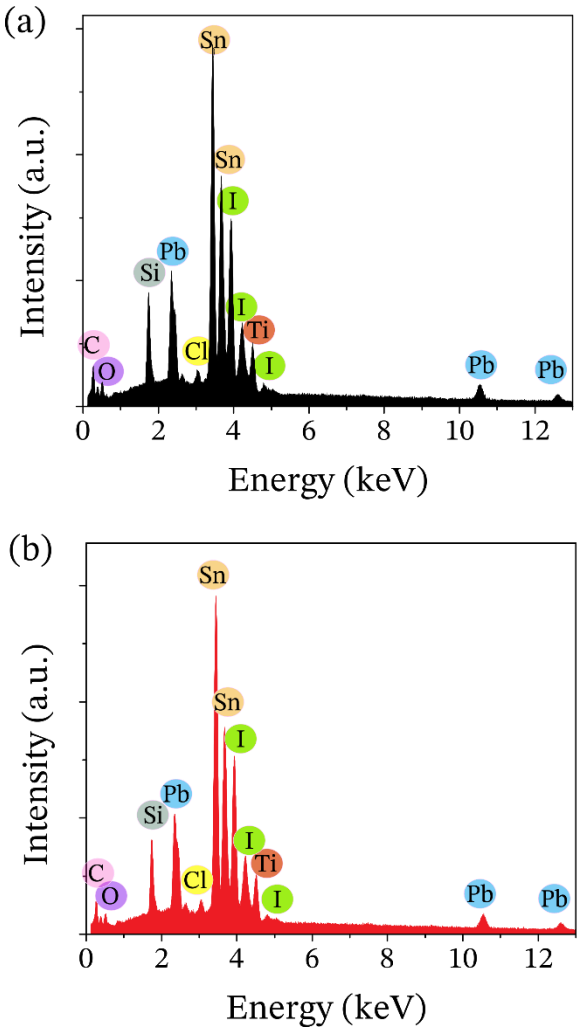

Element	At%
Sn	18.05
I	8.82
Pb	2.92
C	38.41
Si	8.44
N	13.81
O	7.48
Ti	2.07
Cl	0.00

Element	At%
Sn	18.17
I	9.12
Pb	2.81
C	38.01
Si	7.56
N	14.93
O	7.08
Ti	2.29
Cl	0.04

Figure S3. EDX spectra and atomic percentages obtained for $CH_3NH_3PbI_{3-x}Cl_x$ films deposited onto *c*-TiO_2-coated FTO/glass substrates from (a) pristine precursor solution and from (b) a precursor solution containing α-terpineol.

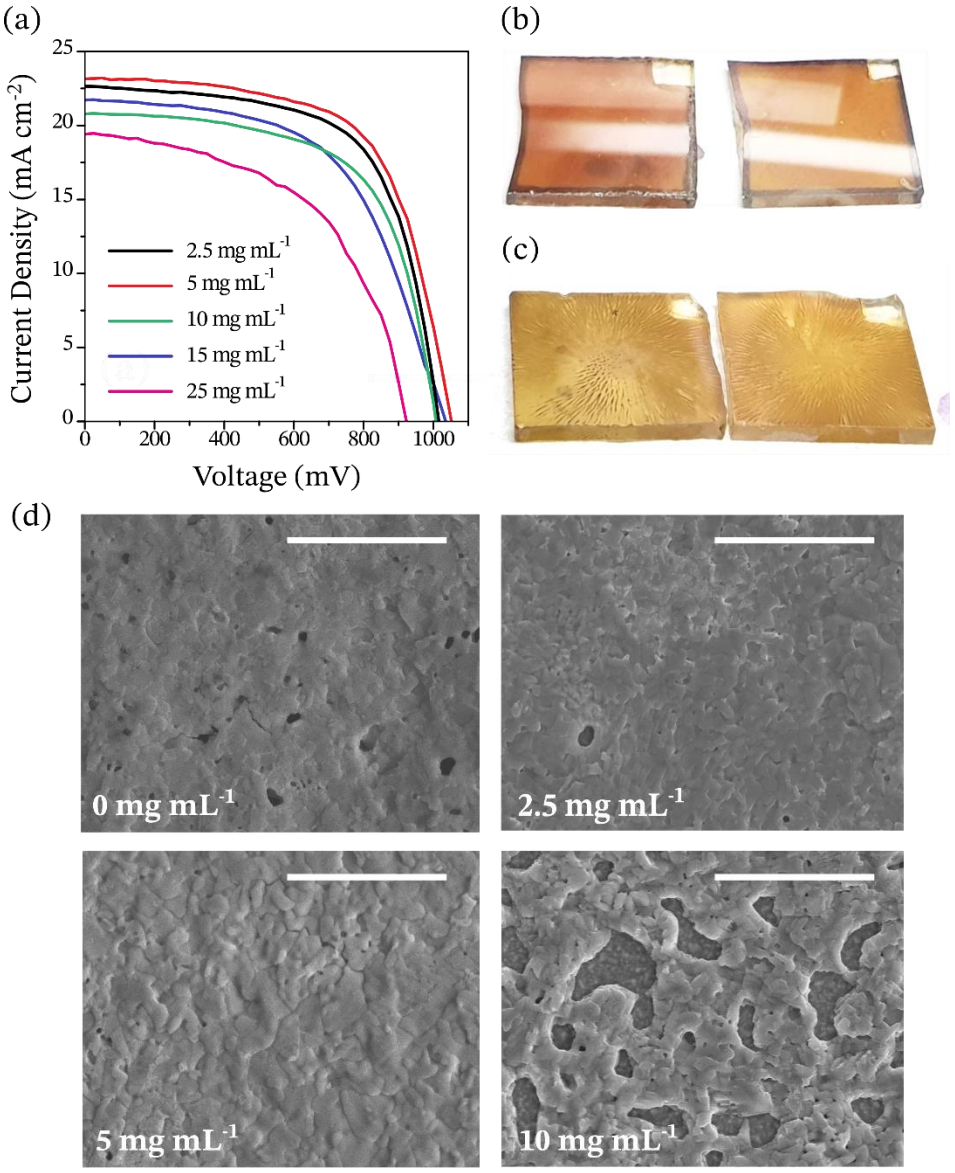

Figure S4. (a) Effect of the α-terpineol additive concentration on the J-V curves of planar n-i-p PSCs. (b) Perovskite precursor films (prior to thermal treatment at 105 °C) obtained by adding 5 mg mL^{-1} of α-terpineol to the one-step precursor solution. (c) Striation defects in perovskite precursor films obtained by adding 25 mg mL^{-1} of α-terpineol to the one-step precursor solution. (d) Top-view SEM images of $CH_3NH_3PbI_{3-x}Cl_x$ perovskite films spin-coated on top of *c*-TiO_2/FTO-coated glass substrates from precursor solutions with different concentration of α-terpineol, namely 0 mg mL^{-1}, 2.5 mg mL^{-1}, 5 mg mL^{-1}, and 10 mg mL^{-1}. Scale bar: 5 μm.

Table S1. Overview on PSC performances (short-circuit current, J_{sc}; open-circuit voltage, V_{oc}; fill factor, FF; power conversion efficiency, PCE) obtained under AM1.5G and reverse voltage scanning direction as a function of the α-terpineol additive concentration in the precursor solution.

Additive Content	J_{sc} [mA cm^{-2}]	V_{oc} [mV]	FF [%]	PCE [%]
0 mg mL^{-1}	23.0	1039	58.2	**13.9**
2.5 mg mL^{-1}	22.7	1015	64.0	**14.7**
5 mg mL^{-1}	23.2	1053	63.1	**15.4**
10 mg mL^{-1}	20.8	1007	62.7	**13.1**
15 mg mL^{-1}	21.7	1035	56.1	**12.6**
25 mg mL^{-1}	19.4	922	53.1	**9.5**

Table S2. Recently reported performances of PSCs based on perovskite films prepared by additive-assisted solution processes, and comparison with our best-efficiency PSCs featuring Ag or Au top electrodes. The power conversion efficiencies (PCEs) of the top pristine and additive-treated PSCs are tabulated basing on data available in each reference. Note that the PSCs fabricated in this work exhibit several advantages over the other devices, including simple planar device architecture, simple one-step spin-coating deposition without the need of antisolvents, and non-toxic, low-cost, and eco-friendly nature of the additive employed.

Additive	Device Architecture	Deposition Method	Additive Properties	PCE *pristine* [%]	PCE *treated* [%]	Ref.
DIO	FTO/PEDOT:PSS/ $MAPbI_3$/PCBM/Ag (planar)	One-step spin-coating + Antisolvent	Toxic (halogenated) High boiling point Interaction through I-atoms	10.77	12.82	[4]

DMSO	FTO/c-TiO_2/mp-TiO_2/ $MAPbI_3$/Spiro-OMeTAD/Au (mesoporous)	Two-step spin-dip method (DMSO in PbI_2 solution)	Percutaneous absorption High boiling point O-donor Lewis base	12.79	17.26	[5]
NMP	FTO/c-TiO_2/mp-TiO_2/ $MAPbI_3$/Spiro-OMeTAD/Au (mesoporous)	Two-step spin-dip method (NMP in PbI_2 solution)	Reproductively toxic High boiling point O-donor Lewis base	13.3	17.5	[6]
HMPA	FTO/c-TiO_2/mp-TiO_2/ $MAPbI_3$/PTAA/Au (mesoporous)	Two-step spin-coating (HMPA in PbI_2 solution) + Antisolvent	Carcinogen High boiling point O-donor Lewis base	18.02	19.5	[7]
Dimethyl-acetamide (DMA)	FTO/c-TiO_2/mp-TiO_2/ $MAPbI_3$/Spiro-OMeTAD/Au (mesoporous)	Two-step spin-coating (DMA in PbI_2 solution)	Reproductively toxic High boiling point O-donor Lewis base	12.32	16.05	[8]
ACN	FTO/c-TiO_2/mp-TiO_2/ $Cs_xFA_{1-x-y}MA_yPb(I_{1-z}Br_z)_3$/ Spiro-OMeTAD/Au (mesoporous)	Two-step spin-coating (ACN in $MA^+/FA^+/Cs^+$ solution)	Modest toxicity Low boiling point Weak coordination	13.06	15.64	[9]
PEG	FTO/c-TiO_2/$MAPbI_{3-x}Cl_x$/Spiro-OMeTAD/Au (planar)	One-step spin-coating No antisolvent	Non-toxic Eco-friendly Low-cost Hydrogen bonding	10.58	13.20	[10]
DMI	FTO/c-TiO_2/mp-TiO_2/ $MAPbI_3$/Spiro-OMeTAD/Au (mesoporous)	Two-step spin-coating (DMI in PbI_2 solution)	Modest toxicity Eco-friendly High boiling point O-donor Lewis base	10.72	14.54	[11]
α-Terpineol	FTO/c-TiO_2/$MAPbI_{3-x}Cl_x$/Spiro-OMeTAD/MoO_x/Ag (**planar**)	**One-step spin-coating** **No antisolvent**	**Non-toxic** **Eco-friendly** **Low-cost** High boiling point Hydrogen bonding	13.9	15.4	**This work**
	FTO/c-TiO_2/$MAPbI_{3-x}Cl_x$/Spiro-OMeTAD/MoO_x/Au (**planar**)			16.1	**17.5**	

Table S3. Degradation of PV parameters (short-circuit current, J_{sc}; open-circuit voltage, V_{oc}; fill factor, FF; power conversion efficiency, PCE) for solar cells processed from solutions with/without α-terpineol and stored in a N_2-filled glove box.

Sample	Storage Time [h]	J_{sc} [mA cm^{-2}]	V_{oc} [mV]	FF [%]	PCE [%]
Without α-terpineol	0	23.0	1039	58.2	**13.9**
	168	20.1	1027	53.0	11.0
	336	19.6	993	52.3	10.2
	504	15.5	984	52.4	8.0
With α-terpineol	0	23.2	1053	63.1	**15.4**
	168	23.6	1018	60.7	14.6
	336	21.8	1035	58.8	13.2
	504	21.1	1006	55.2	11.7

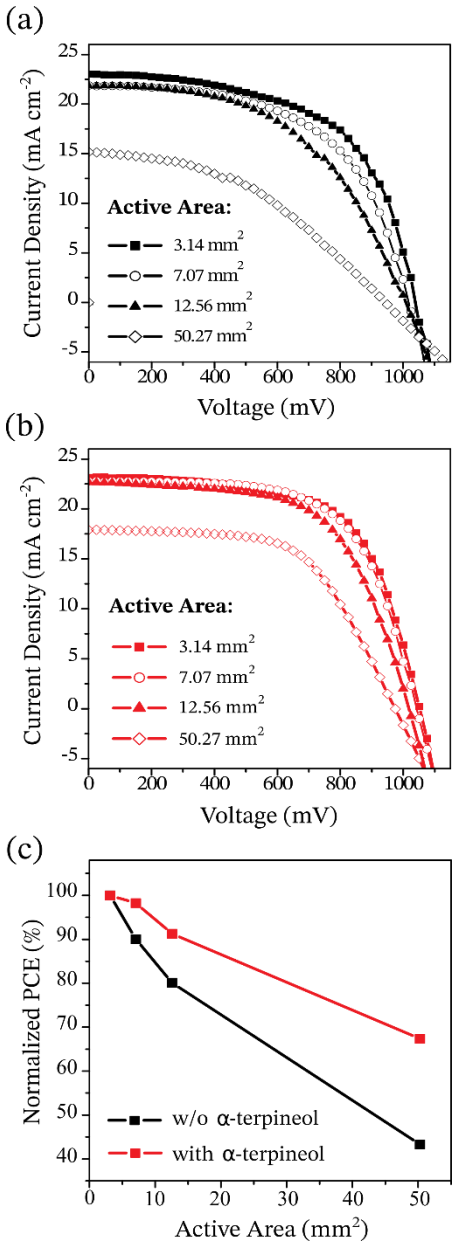

Figure S5. Reverse scanning J-V curves of the best-performance PSCs processed from solutions (a) without α-terpineol and (b) with 5 mg mL^{-1} α-terpineol with increasing of the active area, measured under standard 1 sun illumination. (c) The corresponding variation in PCE with increasing of the active area for pristine and α-terpineol-modified solar cells.

Table S4. Summary of PSC performances for solar cells processed from solutions with/without α-terpineol and featuring different active areas, measured under standard AM 1.5G illumination.

Sample	Active Area [mm^2]	J_{sc} [$mA\ cm^{-2}$]	V_{oc} [mV]	FF [%]	PCE [%]
Without α-terpineol	3.14	23.0	1039	58.2	**13.9**
	7.07	21.9	1018	56.3	12.5
	12.56	21.8	1009	50.6	11.1
	50.27	15.2	943	42.1	6.0
With α-terpineol	3.14	23.2	1053	63.1	**15.4**
	7.07	22.8	1043	63.6	15.1
	12.56	22.7	1018	60.7	14.0
	50.27	17.9	974	59.4	10.4

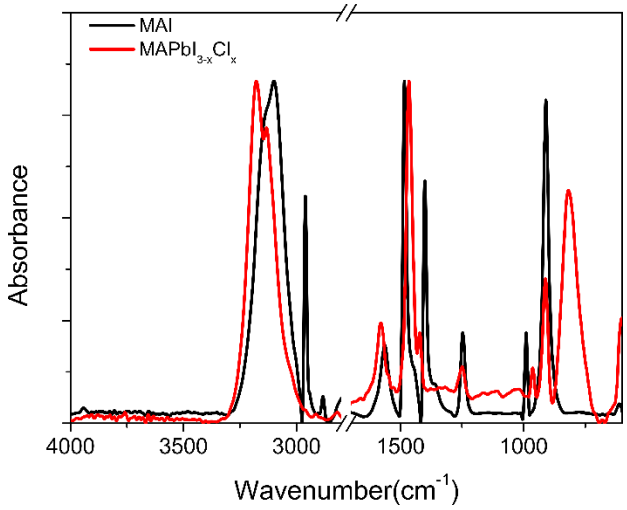

Figure S6. FT-IR spectra registered for: MAI precursor (black line) and a $MAPbI_{3-x}Cl_x$ perovskite layer grown in presence of α-terpineol (red line), prepared in accordance with the general procedure reported in Experimental Section in the main text. For sake of clarity, the spectra have been normalized accordingly to the N-H stretching band intensity (spectral range 4000-2800 cm^{-1}) or to the $N\text{-}H_{sym}$ bending band intensity (spectral range 1700-600 cm^{-1}).

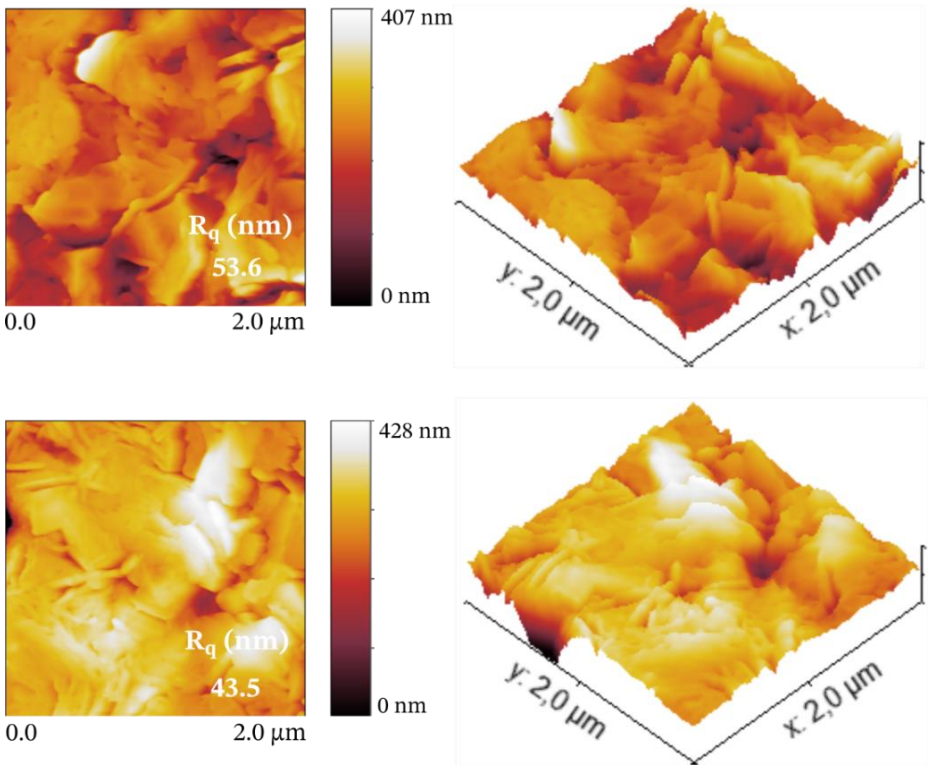

Figure S7. Top-view (left) and 3D (right) AFM images of the pristine perovskite film (above) and of the perovskite film prepared using the α-terpineol additive (below), deposited on top of *c*-TiO_2/FTO/glass substrates. The surface roughness is noted as the root mean-square value (R_q).

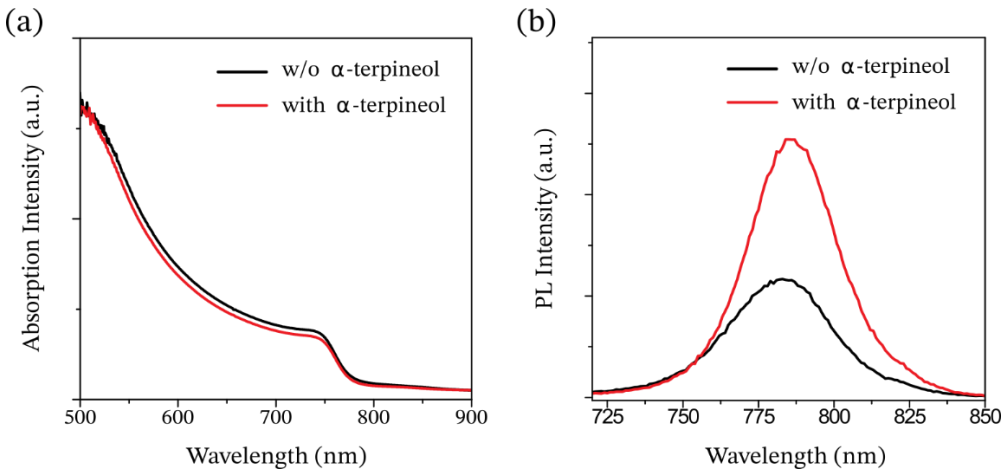

Figure S8. (a) Absorption spectra and (b) steady-state PL spectra of the pristine perovskite films with/without α-terpineol deposited onto FTO/glass substrates.

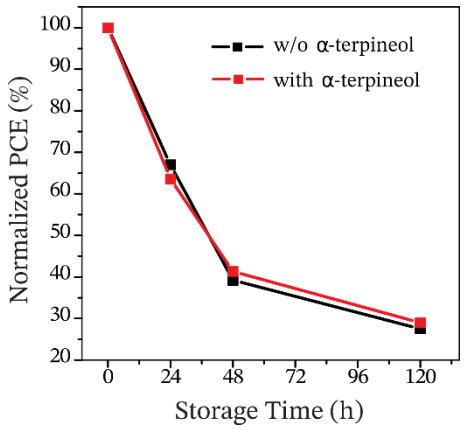

Figure S9. PCE decays of the control and α-terpineol-treated Ag-based devices exposed to ambient air under dark without encapsulation.

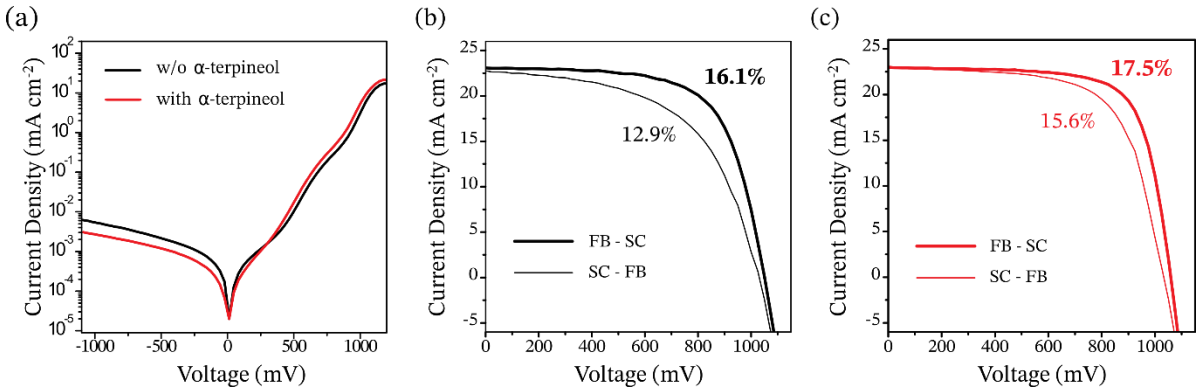

Figure S10. (a) Dark J-V curves (semilog plot) of the best-performance Au-based PSCs processed from solutions with/without α-terpineol. Hysteresis effect in the J-V curves of the top Au-based devices processed from solutions (b) without α-terpineol and (c) with α-terpineol by varying the voltage scanning direction, from forward bias to short-circuit (FB-SC) and from short-circuit to forward bias (SC-FB).

REFERENCES

(1) Ye, M.; He, C.; Iocozzia, J.; Liu, X.; Cui, X.; Meng, X.; Rager, M.; Xiaodan Hong; Liu, X.; Lin, Z. Recent Advances in Interfacial Engineering of Perovskite Solar Cells. *J. Phys. D: Appl. Phys.* **2017**, *50* (37), 373002. https://doi.org/10.1088/1361-6463/aa7cb0.

(2) Sun, Y.; Takacs, C. J.; Cowan, S. R.; Seo, J. H.; Gong, X.; Roy, A.; Heeger, A. J. Efficient, Air-Stable Bulk Heterojunction Polymer Solar Cells Using MoO_x as the Anode Interfacial Layer. *Adv. Mater.* **2011**, *23* (19), 2226–2230. https://doi.org/10.1002/adma.201100038.

(3) Hölzl, J.; Schulte, F. K. Work Function of Metals. In *Solid Surface Physics*; Hölzl, J., Schulte, F. K., Wagner, H., Eds.; Springer Tracts in Modern Physics; Springer Berlin Heidelberg: Berlin, Heidelberg, 1979; pp 1–150. https://doi.org/10.1007/BFb0048919.

(4) Tsai, C.-H.; Lin, C.-M.; Kuei, C.-H. Improving the Performance of Perovskite Solar Cells by Adding 1,8-Diiodooctane in the $CH_3NH_3PbI_3$ Perovskite Layer. *Sol. Energy* **2018**, *176*, 178–185. https://doi.org/10.1016/j.solener.2018.10.037.

(5) Cao, X. B.; Li, C. L.; Zhi, L. L.; Li, Y. H.; Cui, X.; Yao, Y. W.; Ci, L. J.; Wei, J. Q. Fabrication of High Quality Perovskite Films by Modulating the Pb–O Bonds in Lewis Acid–Base Adducts. *J. Mater. Chem. A* **2017**, *5* (18), 8416–8422. https://doi.org/10.1039/C7TA00539C.

(6) Cao, X.; Li, C.; Li, Y.; Fang, F.; Cui, X.; Yao, Y.; Wei, J. Enhanced Performance of Perovskite Solar Cells by Modulating the Lewis Acid–Base Reaction. *Nanoscale* **2016**, *8* (47), 19804–19810. https://doi.org/10.1039/C6NR07450B.

(7) Zhang, Y.; Gao, P.; Oveisi, E.; Lee, Y.; Jeangros, Q.; Grancini, G.; Paek, S.; Feng, Y.; Nazeeruddin, M. K. PbI_2–HMPA Complex Pretreatment for Highly Reproducible and Efficient $CH_3NH_3PbI_3$ Perovskite Solar Cells. *J. Am. Chem. Soc.* **2016**, *138* (43), 14380–14387. https://doi.org/10.1021/jacs.6b08347.

(8) Cao, X.; Zhi, L.; Li, Y.; Fang, F.; Cui, X.; Yao, Y.; Ci, L.; Ding, K.; Wei, J. Elucidating the Key Role of a Lewis Base Solvent in the Formation of Perovskite Films Fabricated from the Lewis Adduct Approach. *ACS Appl. Mater. Interfaces* **2017**, *9* (38), 32868–32875. https://doi.org/10.1021/acsami.7b07216.

(9) Hussein, H. T.; Zamel, R. S.; Mohamed, M. S.; Mohammed, M. K. A. High-Performance Fully-Ambient Air Processed Perovskite Solar Cells Using Solvent Additive. *J. Phys. Chem. Solids* **2021**, *149*, 109792. https://doi.org/10.1016/j.jpcs.2020.109792.

(10) Chang, C.-Y.; Chu, C.-Y.; Huang, Y.-C.; Huang, C.-W.; Chang, S.-Y.; Chen, C.-A.; Chao, C.-Y.; Su, W.-F. Tuning Perovskite Morphology by Polymer Additive for High Efficiency Solar Cell. *ACS Appl. Mater. Interfaces* **2015**, *7* (8), 4955–4961. https://doi.org/10.1021/acsami.5b00052.

(11) Zhi, L.; Li, Y.; Cao, X.; Li, Y.; Cui, X.; Ci, L.; Wei, J. Perovskite Solar Cells Fabricated by Using an Environmental Friendly Aprotic Polar Additive of 1,3-Dimethyl-2-Imidazolidinone. *Nanoscale Res. Lett.* **2017**, *12* (1), 632. https://doi.org/10.1186/s11671-017-2391-3.